

Comparison of Narrow Bipolar Events with ordinary lightning as proxies for the microwave-radiometry ice-scattering signature

Abram R. Jacobson^{1,2}, William Boeck^{3,2}, and Christopher Jeffery²

¹ University of Washington, Seattle, Washington

² Los Alamos National Laboratory, Los Alamos, New Mexico

³ Niagara University, Lewiston, New York

to be submitted to Monthly Weather Review

Corresponding author:

Abram R. Jacobson

abramj@u.washington.edu

(360)734-5019

ABSTRACT

The Narrow Bipolar Event (NBE) is a unique lightning discharge that has a short (~ 10 μs) overall duration, that lacks a prior leader phase, and that produces too little light output to be visible by optical lightning detectors on satellites. NBEs thus have basic differences from ordinary lightning discharges, which occur in flashes lasting up to a fraction of a second, which carry significant current in a “stroke” only after a leader stage which prepares the conductive channel, and which produce copious light that is recordable from space. Thus we are motivated to determine whether the meteorological setting of NBEs differs from, or is similar to, that of ordinary lightning. A previous paper started this project of comparing NBE/ordinary lightning, by comparing the placement of either type of lightning within spatial structures of cloud depth, as revealed by infrared cloud-top temperature. That previous study employed lightning data from the Los Alamos Sferic Array (LASA) in Florida. The present paper extends this approach to comparing LASA NBE/ordinary lightning events’ spatial relationships to radiometric cloud imagery from the TRMM (Tropical Rainfall Measurement Mission) Microwave Imager (TMI) 85-GHz channels. This form of radiometric imagery reveals the location of deep, active convective cores with more acute spatial selectivity than does the infrared cloud-top temperature. We find that the behaviors of NBEs and ordinary lightning are, once again, indistinguishable, but with regard this time to proximity to deep convective cores as revealed by TMI.

1. INTRODUCTION

The Narrow Bipolar Event (NBE) is a unique intracloud lightning discharge that has been studied both with ground-based (Smith et al. 1999; Suszcynsky and Heavner 2003; Jacobson and Heavner 2005) and satellite-based (Holden et al. 1995; Massey and Holden 1995; Massey et al. 1998; Light and Jacobson 2002; Jacobson 2003b; 2003a; Jacobson and Light 2003) radio and optical instruments. Observations (Gurevich et al. 1999; Light and Jacobson 2002; Jacobson 2003a; 2003b; Jacobson and Light 2003) and conceptual models (Gurevich et al. 1999) suggest that NBEs arise from physical processes different from those in ordinary lightning. First, NBEs are sudden, fast (duration $\sim 10 \mu\text{s}$) intracloud discharges that *entirely lack the preliminary leader phase* seen in “ordinary” lightning (Smith et al. 1999; Jacobson 2003b). Second, NBEs lack optical emissions of sufficient intensity to be visible from the same space-borne optical lightning detectors (Light and Jacobson 2002) which routinely monitor ordinary lightning. Obviously this indicates that NBEs are different from ordinary lightning, whose very name (“lightning”) indicates optical visibility. Therefore it is important to test whether NBEs occur in similar meteorological environments as do ordinary lightning discharges. This paper is the final of a series describing such tests, using satellite remote-sensing imagery to classify cloud conditions near NBEs, as compared with cloud conditions near ordinary lightning in the same observing campaign.

Two previous papers (Suszcynsky and Heavner 2003; Jacobson and Heavner 2005) studied the relationship of NBEs to ordinary lightning using the ground-based Los Alamos Sferic Array (LASA) vertical-electric-field-change array in Florida (Smith et al.

2002; Jacobson 2003a). One of these papers (Jacobson and Heavner 2005) also compared LASA-detected lightning to GOES-East infrared (IR; 10.7-micron) cloud imagery. That study, subsequently referred to as “JH2005”, showed a strong association between lightning incidence (as seen by LASA) and high (and therefore cold) cloud tops as inferred from IR blackbody brightness temperature. JH2005 showed that NBEs behaved substantially the same as does ordinary lightning, in terms of spatial relationship to 10.7-micron cloud-top temperature features.

The present paper extends the approach of JH2005 to comparing NBEs with spatial features in microwave radiometric imagery of clouds. Satellite-based microwave radiometry relies for its interpretation on complex radiative transfer and forward-modeling calculations (Spencer et al. 1989; Smith et al. 1992; Kummerow and Giglio 1994a; 1994b; Prigent et al. 2001; Wiedner et al. 2004). Unlike the 10.8-micron cloud-top brightness temperature, the microwave signal lacks a straightforward interpretation and requires significant supporting theory and modeling.

However, one opportunistic product of microwave radiometry is used qualitatively to indicate the presence of large ice water paths of precipitation-size ice: the “ice-scattering signature”, based on 85-GHz channels in the case of TRMM. The ice-scattering signature is so named because it is due to ice-hydrometeor scattering, from the radiometer line-of-sight, of upwelling radiation emitted in the lower troposphere mainly by liquid hydrometeors (Nesbitt et al. 2000). The ice-scattering signature is a depression in the radiance reaching the radiometer, or, in terms of brightness temperature, as a brightness-

temperature depression. It is somewhat arbitrary which threshold to choose for an “ice-scattering signature”. Criteria have been chosen by other investigators (Mohr and Zipser 1996) for identifying storm types and to define “intense ice scattering” thresholds in microwave-radiometer imagery. In general, brightness-temperature depressions to the region $T < 170$ K are associated with the active cores of significant, deep convection. We stress that *the depressed apparent temperature is not a kinetic temperature*. Rather, the cloud system is not optically thick, so the brightness temperature cannot be interpreted in terms of the local cloud-top properties. The scattering out of the line-of-sight is due to precipitation-sized ice, mainly graupel, in the upper portion of the thunderstorm. The ice-scattering signature thus marks the presence of localized enhanced ice water path aloft. It has recently been shown, also on the basis of TRMM, that the vertically-integrated ice-water-path is the most robust column-integrated correlate of lightning (Petersen et al. 2005).

The correspondence between ordinary lightning and ice-scattering signatures has been robustly demonstrated by several authors via comparison of TRMM-based LIS data and TMI imagery (Nesbitt et al. 2000; Toracinta and Zipser 2001; Ushio et al. 2001; Toracinta et al. 2002; Ushio et al. 2002). Those authors showed that high lightning flash rates tend to occur in regions of deeply depressed polarization-corrected 85-GHz apparent brightness temperature (PCT).

Because NBEs have been found to lack optical output sufficiently powerful to be detectable from space (Light and Jacobson 2002), there has not been any satellite-optical

study of the relationship of NBEs to the ice-scattering signature, and nor is there likely to be. To fill this void, we document the relationship of TMI ice-scattering signatures to both ordinary and NBE lightning discharges observed by LASA.

2. METHOD

LASA's key contribution to this study is its ability to detect and to identify NBE discharges (Smith et al. 2002; Smith et al. 2004). This is done by detailed examination of the archived waveform (see JH2005). The LASA Florida region, through the year 2002, is shown in Figure 1. It is centered at 28 deg N and -81.5 deg E. (The array effective center more recently changed slightly for 2004 *et seq.*) Also shown is a 400-km-radius circle, within which reliable lightning locations and characterizations are readily achieved by LASA (Smith et al. 2002; Jacobson and Heavner 2005). In this study we will limit our attention to lightning lying within this circle. The LASA stations used in this study are listed in Table 1. The LASA detection efficiency within the 400-km study radius is not precisely known, but is believed on the basis of previous studies to exceed 80% for both cloud-to-ground and intracloud lightning discharges (Smith et al. 2002).

The TRMM satellite track controls the curved image swaths of the VIRS infrared imager and the TMI microwave radiometer. These image swaths irregularly and usually only partially overlap with the Florida study region. The VIRS 10.8-micron-wavelength (i.e., Channel 4) image is formed by the detector sweeping along a line orthogonal to the satellite track, while the TMI image is formed by the detector swinging at constant nadir angle around 360 degrees of azimuth (in the satellite frame) (Kummerow et al. 1998).

The VIRS image swath is 720 km wide, while the TMI image swath is 759 km wide (with the original orbital altitude of 350 km). Obviously, neither the VIRS nor the TMI native data pixels simply coincide with our Earth-fixed E-W/N-S axis system used by LASA. Therefore we have chosen to resample both the VIRS and TMI data onto an Earth-fixed pixel array whose axes coincide with Eastward and Northward, centered at the LASA array center (28 N, -81.5 E). The resampling grid covers 8degX8deg, in 0.01-deg steps. This step size is much smaller than the VIRS and TMI imager native pixel sizes but is convenient for the graphical and correlation analysis to follow. Each time that the narrower image swath, that of VIRS, even partially overlaps with the 400-km-radius lightning-data circle (see Figure 1), we store the VIRS and TMI resampled pixel values for comparison with lightning. We attempt to ensure that the lightning that spatially overlaps a cloud feature is due to the same cloud configuration imaged by the satellite, by requiring the lightning to occur no more than 15 minutes from the time that TRMM passes over -81.5 deg E (the array-center meridian).

The native VIRS and TMI pixels are georeferenced to ground level, but we are concerned with cloud phenomena occurring above ground height, i.e. in the height region of mixed-phase microphysics. The TMI data, which are taken at constant incidence angle (Kummerow et al. 1998), can be readily shifted so they are georeferenced to cloud height. We choose 10-km altitude as a standard cloud height to which to georeference the TMI data. The choice of 10 km is due to its proximity to the height of the ice-scattering process.

Of the several TMI wavelengths, we use data only from 85-GHz. That channel is recorded in two separate polarizations, horizontal and (quasi-)vertical. We use a linear combination of the 85-GHz vertical and horizontal polarization signals, known as the “polarization-corrected temperature” (PCT), that is empirically optimized to minimize ground-emission contrast between land and sea under clear-sky conditions (Weinman and Guetter 1977). Using PCT removes from the images most residual structure due to the land/sea contrast in direct ground-level emission. However, use of PCT for the present purpose- locating columns of precipitation-size ice -is not strictly necessary, because in the regions with deep cloud cover, the ground is occluded anyway, and the emission is dominated by hydrometeors in the lower troposphere rather than by the ground (Spencer et al. 1989; Smith et al. 1992; Kummerow and Giglio 1994b; Prigent et al. 2001; Wiedner et al. 2004).

Figure 2 shows (a) resampled VIRS imagery and (b) resampled TMI PCT for a typical TRMM pass. The brightness-temperature scales differ for the two instruments. For VIRS, the brightness temperature approximates the cloud-top kinetic temperature, because of the cloud’s great optical depth for 10.8-micron wavelength radiation. For TMI, on the other hand, the PCT is not a simple blackbody emission but rather is due to emission low in the atmosphere convolved with emission and, more importantly, scattering (by precipitation-size ice) higher in the atmosphere (Mohr et al. 1999; Nesbitt et al. 2000; Toracinta and Zipser 2001; Toracinta et al. 2002). Figure 2 also shows overlaid lightning events occurring within ± 15 minutes of the satellite pass. The small square symbols are non-NBEs, while the sole large triangle is an NBE. It can be seen that

the lightning events in this example tend to be clustered near the depressed-PCT ice-scattering signatures. It is obvious that the TMI PCT is a far closer and more selective correlate of the occurrence of lightning than is the VIRS cloud-top temperature. This is not surprising, in view of the fact that thunderstorm electrification requires robust mixed-phase microphysical processes that do not occur in, e.g., cirrus shields (another contributor to VIRS cold cloud tops).

Because the LASA array is fixed on the ground, while the TRMM satellite is in low-Earth orbit, we obtain only sporadic and transient TRMM coverage over portions of the LASA lightning-location region. Consequently, this report includes much less cumulative observation time than did JH2005, which employed data from geostationary-satellite staring IR images that were (in principle) perennially available over the LASA location. This results in there being approximately 30 times fewer lightning events seen by LASA during TRMM overpasses than were available during the geostationary-imager campaign described in JH2005, during the same overall study period (1999-2002). Moreover, the requirement for temporal coincidence (within ± 15 minutes) with TRMM overflights effectively cut our study period down from four to three years, 2000-2002, because LASA was not run as intensively during 1999 as during the subsequent three years. In terms of lightning events for which we have supporting VIRS and TMI imagery, we have a total of only 39,312 non-NBE lightning events, and only 1769 NBEs. These are distributed over 568 "scenes" of joint VIRS/TMI imagery. We include in this 568 only those image scenes accompanied by at least one (1) LASA lightning event. We stress

that most of the 568 images (as in the example of Figure 2) only partially overlap with the 400-km-radius circle of lightning observations.

In next section, we will compare non-NBE and NBE lightning statistics. The approach will be to compare histograms of those lightning types' behaviors with respect to cloud-radiometric properties. We compute the standard Kolmogorov-Smirnov (K-S) test statistic (Press et al. 1995) in case the reader would like use that statistic to determine whether any two distributions are significantly similar or different. In each such case, we compare distributions of brightness temperatures in the vicinity of non-NBEs and NBEs. Each native pixel is an independent radiometric measurement. The native pixels (Kummerow et al. 1998) for either VIRS or TMI (85 GHz) are about 32 times the area of the resampled pixels used here (see above). *This article's subdivision of a native pixel into 32 resampled pixels does not produce any new statistical degrees of freedom.* Thus, in compiling the K-S statistic, we count the effective number of *native*, not resampled pixels, in the vicinity of the lightning events. However, we work in resampled pixels. Thus we correct to the effective number of *native* pixels by dividing the number of resampled pixels by 32.

The K-S statistic is estimated as follows. Let M be the number of native pixel radiometric measurements near non-NBE lightning. Let N be the number of native pixel radiometric measurements near NBE lightning. Let H_M be the normalized, cumulative distribution of brightness temperature near non-NBE lightning. Let H_N be the normalized, cumulative

distribution of brightness temperature near NBE lightning. Then the K-S statistic (Press et al. 1995) is defined as

$$K = [2MN/(M+N)]^{1/2} \max(|H_M - H_N|) \quad \text{Eq. (1)}$$

The rest of this article will deal with overall statistics from the hundreds of image sets similar to the example of Figure 2.

3. STATISTICAL RESULTS

3a. VIRS/LASA comparison

These results regarding VIRS largely confirm the results reported earlier in JH2005, which were based on comparison of GOES-East 10.7-micron imagery with LASA lightning data. Therefore these VIRS results will be described only briefly and as an introduction to the TMI results (Section 3b below).

Figure 3 shows distributions of VIRS 10.8-micron brightness temperature for the all the scenes containing LASA lightning. The thin solid curve is the brightness-temperature distribution for all scene pixels, regardless of whether lightning occurs in or near the pixel. The two thick curves are also distributions of brightness temperatures, but conditioned for lightning-proximal pixels only, within 30 km (solid curve), and 100 km (dashed curve), of LASA non-NBE lightning. The VIRS-LASA comparison thus shows that cloud-top temperature close to lightning is peaked near 205 K, which is very cold compared to the all-scene distribution (thin solid curve.) These results are almost identical to GOES/LASA results reported in JH2005's Figure 9(a).

Figure 4 is similar to Figure 3 but for LASA NBEs. Comparison of Figure 4 with Figure 3 above shows that NBEs are at least as selective for cold cloud-top temperatures as are non-NBEs. As to whether NBEs differ from non-NBEs the K-S statistics (see Eq. 1) are $K = 4.9 \times 10^1$ and 1.2×10^2 for 30-km and 100-km radii, respectively. Thus according to the high value of K, the NBEs' increased selectivity for cold cloud-top temperatures is statistically significant. Figure 4 is almost identical to GOES/LASA results reported in JH2005's Figure 9(b). Apparently the cloud environment around NBEs is similar to the cloud environment around non-NBEs, at least according to this measure.

Figures 5 and 6 are analogous, respectively, to Figures 3 and 4, except that the distributions shown in heavy curves are for the *minimum* brightness temperatures within 30 km (solid curve) and 100 km (dashed curve) of LASA lightning events. The minimum temperature is only rarely above 225 K, and the distribution peaks in the range 200 K or even colder. As to whether NBEs differ from non-NBEs the K-S statistics (see Eq. 1) are $K = 1.5$ and 1.7 for 30-km and 100-km radii, respectively. These values of K are less clear-cut, so it is proper only to say that NBEs' proximal minimum cloud-top temperatures do not significantly differ from those of non-NBEs. The results of Figure 5 and 6 are almost identical to the GOES/LASA results reported in JH2005's Figure 10.

The results so far (Figures 3-6) describe the cloud-top temperatures that are *necessary* for the occurrence of lightning. On the basis of these results, we can state with some confidence that lightning in Florida requires cloud-top temperatures that are low enough

(< 225 K) to imply cloud-top heights exceeding 10 km (see JH2005's Figure 7). This is consistent with the necessary mixed-phase-microphysical conditions for cloud electrification (Williams 1985; 2001; Petersen et al. 2005).

This question can be turned around: To what extent does lightning serve as a proxy for cold cloud-top temperatures? The answer is expected to be that lightning is only a very weak proxy, because cold cloud-top temperatures can be created not only by convective cores, but also by anvil shields that are relatively free of lightning (Molinie and Jacobson 2004; Jacobson and Heavner 2005).

In Figure 7 we address this question with VIRS and lightning data. We take all pixels and display their brightness temperature distribution (dashed curve). Next, we subtract, from this overall set, any pixels that are within 30 km of at least one contemporaneous LASA lightning event. Thus we are "cutting-out" those regions of the VIRS scenes that are close to lightning. This "cut-out" distribution is shown as the solid curve in Figure 7. We do not split this exercise into non-NBE and NBE lightning separately, because our small number of lightning events does not provide sufficient sampling. Thus the cut-out distribution, in the solid curve, is for proximity to all lightning, regardless of the type. At warmer temperatures (> 245), the cut-out and overall distributions are almost indistinguishable. This is because lightning does not occur at such elevated temperatures, i.e., within clouds with such modest implied cloud-top heights. As the temperature decreases below 245 K, the cut-out distribution is progressively depressed, relative to the overall distribution. At the coldest temperature bin (194 K), Figure 7 shows that > 60%

of the pixels lie within 30 km of lightning, but this decreases to 50% at only 10 K or one bin warmer, where most lightning occurs (see Figure 3 above). Thus, lightning does not serve as a reliable proxy for the cloud regions having the coldest 10.8-micron brightness temperatures. This is consistent with our expectations from prior experience (Molinie and Jacobson 2004; Jacobson and Heavner 2005) based on GOES-East 10.7-micron imagery.

3b. TMI/LASA comparison

We now show analogous TMI/LASA comparisons as were just performed for VIR/LASA. Figure 8, which is analogous to Figure 3, shows the distribution of 85-GHz PCT over the 568 scenes in our archive. The thin solid curve is the background distribution, comprising all pixels in the scenes. It is heavily peaked at the highest temperatures and monotonically decreases toward low temperatures. This is due to the fact that the ice-scattering signature is present in only the deep, active convection cores in which precipitation-size ice is concentrated aloft (Petersen et al. 2005), and such cores cover only a small fraction of the viewed area. The heavy curves show the PCT for pixels within 30 km (solid curve) and within 100 km (dashed curve) of LASA non-NBEs. These curves are enhanced at low temperatures compared to the background curve (more for the 30-km curve, less for the 100-km curve), but they still peak at high temperatures, and still monotonically decrease as the temperature is lowered. This indicates that the PCT depressions- that is, the ice-scattering signatures -occur over small areas that are localized to the lightning, such that even the 30-km radius circle around each lightning event tends to include a significant fraction of pixels that do not exhibit the ice-scattering signature.

This is in marked contrast to the behavior of 10.8-micron brightness-temperature distributions in the neighborhood of lightning, in which lightning occupies a small subset of a relatively vast and undifferentiated cold cloud top. Indeed, the well-known spatial selectivity of 85-GHz PCT for ice aloft is its key advantage in monitoring from space the location and intensity of deep convective cores (Mohr et al. 1999; Nesbitt et al. 2000; Toracinta and Zipser 2001; Toracinta et al. 2002).

Figure 9 is similar to Figure 8 but is for LASA NBEs. Comparing Figure 9 with Figure 8 indicates that the cloud environment around NBEs is similar to the cloud environment around non-NBEs, at least according to this measure. As to whether NBEs differ from non-NBEs the K-S statistics (see Eq. 1) are $K = 1.9 \times 10^1$ and 3.2×10^1 for 30-km and 100-km radii, respectively. These elevated values of K indicate that NBEs have significantly increased selectivity for 85-GHz PCT depressions.

We now examine statistics on the *coldest PCT* in the vicinity of LASA lightning. Figures 10 and 11 present the 85-GHz/LASA relationship for non-NBEs and for NBEs, respectively, analogous to the 10.8-micron/LASA relationship from Figures 5 and 6. As to whether NBEs differ from non-NBEs the K-S statistics (see Eq. 1) are $K = 1.5$ and 1.7 for 30-km and 100-km radii, respectively. This is not clear-cut evidence for a different behavior between NBEs and non-NBEs. Figures 10 and 11 show that there is likely to be an extremely depressed PCT in proximity to lightning, although the distribution of all pixels in proximity to lightning (Figures 8 and 9) is far warmer. This PCT behavior is qualitatively different from the 10.8-micron brightness-temperature behavior, in which

the distribution of coldest pixel temperature (Figures 5 and 6) differs less radically from the distribution of proximal pixels (Figures 3 and 4). With the PCT distributions, the coldest-pixel behavior is almost reversed from the proximal-pixel behavior: The coldest-pixel distribution peaks at lowest temperature and (more or less) monotonically decreases as the temperature increases.

With regard to NBE versus non-NBE differences, Figures 8-11 indicate that NBEs are at least as likely to be in proximity to an ice-scattering signature as are non-NBEs. Thus, in a manner similar to what we saw with the 10.8-micron/LASA comparison, NBEs and non-NBEs occur in similar cloud environments, at least according to each of these two radiometric measures.

Finally, in Figure 12 we calculate the “cut-out” distribution for the TMI 85-GHz PCT. The dashed curve, or background, is for all pixels, without reference to lightning. The solid curve is similar, but after cutting-out the pixels within 30 km of any LASA lightning. This cut-out curve is lower than the background curve, by an amount that increases as the PCT is reduced. The cut-out depression at $PCT < 145$ K is approximately 80%. This means that for $PCT < 145$ K, LASA lightning in the epoch 2000-2002 serves as a proxy for ice-scattering signatures with about 80% efficiency. *That high efficiency is obtained only by using all LASA lightning.* The efficiency using only NBEs would be very low, below 10%, because of NBEs’ low occurrence rate compared to overall lightning. It is as yet undetermined how efficient a proxy will be provided by an NBE-

related phenomenon, the strong very-high-frequency (VHF; 30-300 MHz) in-cloud lightning emissions that can be observed from space (Suszcynsky et al. 2000).

The lightning/ice-scattering-signature efficiency will certainly be enhanced by use of a more sensitive lightning-detection system, such as the planned staring lightning imager to be deployed on a future GOES geostationary satellite (Christian et al. 1989). However, that methodology will not include NBEs, as their luminosity is too weak to be detected from space.

Even at 80%, however, the LASA lightning/PCT proxy efficiency is higher than is the lightning/10.8-micron-cold-cloud-top proxy efficiency seen earlier in Figure 7. This is due to the selectivity of the ice-scattering signature, relative to mere cold cloud tops, for the microphysical environment required for thunderstorm electrification (Petersen et al. 2005).

4. CONCLUSIONS

We have presented statistical results relating LASA-detected lightning to spatial features in TRMM/VIRS and TRMM/TMI radiometric cloud images. The VIRS results, in which the image brightness temperature is a good measure of cloud-top height, largely recap earlier results seen with GOES-East 10.7-micron images (JH2005).

The TMI results, on the other hand, are the first results capable of comparing the proximity of spatial features of the ice-scattering signature to *both* ordinary lightning and NBEs. We find the following:

(a) Both ordinary lightning and NBEs have a similar affinity for depressed-PCT cloud regions.

(b) Despite this affinity for low PCT, the 30-km-radius neighborhood around either an ordinary or an NBE lightning event is a mixture of deeply depressed PCT (e.g, < 145 K) and higher PCT. This is indicative of the smaller spatial scales (~10 km) of intense convective cores compared to cold-cloud-top regions.

(c) Despite this mixture, the *lowest* PCT value within 30 km of either an ordinary or an NBE lightning event is likely to be depressed below 145 K. This implies that NBEs, like ordinary lightning, occur within, or closely neighboring, intense convective cores with enhanced ice water path.

(d) LASA sees too few NBEs for NBEs to provide a close spatial proxy of TMI ice-scattering signatures. LASA sees enough overall lightning (ordinary plus NBE) to provide an 80%-efficient proxy of ice-scattering signatures having a PCT < 145 K.

Acknowledgements

This work was performed under the auspices of the United States Department of Energy. The TRMM TMI and VIRS data were kindly provided by the National Aeronautics and Space Administration (NASA), via the Goddard Space Flight Center DAAC internet portal. The authors are indebted to Dr. C. Kummerow for useful discussions on the TMI data. We also appreciate the insightful comments by the reviewer.

References

Christian, H. J., R. J. Blakeslee, and S. J. Goodman, 1989: The detection of lightning from geostationary orbit. *J. Geophys. Res.*, **94**, 13,329-13,337.

Gurevich, A. V., K. P. Zybin, and R. A. Roussel-Dupré, 1999: Lightning initiation by simultaneous effect of runaway breakdown and cosmic ray showers. *Phys. Lett.*, **A254**, 79-87.

Holden, D. N., C. P. Munson, and J. C. Devenport, 1995: Satellite observations of transionospheric pulse pairs. *Geophys. Res. Lett.*, **22**, 889-892.

Jacobson, A. R., 2003a: Relationship of intracloud-lightning radiofrequency power to lightning-storm height, as observed by the FORTE satellite. *J. Geophys. Res.*, **108**, 4204, doi:10.29/2002JD002956.

— —, 2003b: How do the strongest radio pulses from thunderstorms relate to lightning flashes? *J. Geophys. Res.*, **108**, 4778, doi:10.1029/2003JD003936.

Jacobson, A. R. and T. E. L. Light, 2003: Bimodal radiofrequency pulse distribution of intracloud-lightning signals recorded by the FORTE satellite. *J. Geophys. Res.*, **108**, 4266, doi:10.1029/2002JD002613.

Jacobson, A. R. and M. J. Heavner, 2005: Comparison of Narrow Bipolar Events with ordinary lightning as proxies for severe convection. *Mon. Wea. Rev.*, **133**, 1144-1154.

Kummerow, C. and L. Giglio, 1994a: A passive microwave technique for estimating rainfall and vertical structure information from space. Part I: Algorithm description. *J. Appl. Meteorol.*, **33**, 3-18.

— —, 1994b: A passive microwave technique for estimating rainfall and vertical structure information from space. Part II: Application to SSM/I data. *J. Appl. Meteorol.*, **33**, 19-34.

Kummerow, C., W. Barnes, T. Kozu, J. Shiue, and J. Simpson, 1998: The Tropical Rainfall Measuring Mission (TRMM) sensor package. *J. Atmos. Oceanic Technol.*, **15**, 809-817.

Light, T. E. L. and A. R. Jacobson, 2002: Characteristics of impulsive VHF lightning observed by the FORTE satellite. *J. Geophys. Res.*, **107**, 4756, doi:1029/2001/JD001585.

Massey, R. S. and D. N. Holden, 1995: Phenomenology of transionospheric pulse pairs. *Radio Sci.*, **30**, 1645-1659.

Massey, R. S., D. N. Holden, and X.-M. Shao, 1998: Phenomenology of transionospheric pulse pairs: Further observations. *Radio Sci.*, **33**, 1755-1761.

Mohr, K. I. and E. J. Zipser, 1996: Mesoscale convective systems defined by their 85-GHz ice scattering signature: Size and intensity comparison over tropical oceans and continents. *Mon. Weath. Rev.*, **124**, 2417-2437.

Mohr, K. I., J. S. Famiglietti, and E. J. Zipser, 1999: The contribution of tropical rainfall with respect to convective system type, size, and intensity estimated from the 85-MHz ice-scattering signature. *J. Appl. Meteor.*, **38**, 596-606.

Molinie, G. and A. R. Jacobson, 2004: Cloud-to-ground lightning and cloud top brightness temperature over the contiguous United States. *J. Geophys. Res.*, **109**, D13106, doi:10.1029/2003JD003593.

Nesbitt, S. W., E. J. Zipser, and D. J. Cecil, 2000: A census of precipitation features in the tropics using TRMM: Radar, ice scattering, and lightning observations. *J. Climate*, **13**, 4087-4106.

Petersen, W. A., H. J. Christian, and S. A. Rutledge, 2005: TRMM observations of the global relationship between ice water content and lightning. *Geophys. Res. Lett.*, **32**, doi:10.1029/2005GL023236.

Press, W. H., S. A. Teukolsky, W. T. Vetterling, and B. P. Flannery, 1995: *Numerical Recipes in C*. Cambridge University Press.

Prigent, C., J. R. Pardo, M. I. Mishchenko, and W. B. Rossow, 2001: Microwave polarized signatures generated within cloud systems: Special Sensor Microwave Imager (SSM/I) observations interpreted with radiative transfer simulations. *J. Geophys. Res.*, **106**, 28,243-28,258.

Smith, D. A., X. M. Shao, D. N. Holden, C. T. Rhodes, M. Brook, P. R. Krehbiel, M. Stanley, W. Rison, and R. J. Thomas, 1999: A distinct class of isolated intracloud lightning discharges and their associated radio emissions. *J. Geophys. Res.*, **104**, 4189-4212.

Smith, D. A., K. B. Eack, J. Harlin, M. J. Heavner, A. R. Jacobson, R. S. Massey, X. M. Shao, and K. C. Wiens, 2002: The Los Alamos Sferic Array: A research tool for lightning investigations. *J. Geophys. Res.*, **107**, 10.1029/2001JD000502.

Smith, D. A., M. J. Heavner, A. R. Jacobson, X. M. Shao, R. S. Massey, R. J. Sheldon, and K. C. Wiens, 2004: A method for determining intracloud lightning and ionospheric heights from VLF/LF electric field records. *Radio Sci.*, **39**, doi:10.1029/2002RS002790.

Smith, E. A., A. Mugnai, H. J. Cooper, G. J. Tripoli, and X. Xiang, 1992: Foundations for statistical-physical precipitation retrieval from passive microwave satellite measurements. Part 1: Brightness-temperature properties of a time-dependent cloud-radiation model. *J. Appl. Meteorol.*, **31**, 506-531.

Spencer, R. W., H. M. Goodman, and R. E. Hood, 1989: Precipitation retrieval over land and ocean with the SSM/I: Identification and characteristics of the scattering signal. *J. Atmos. Oceanic Technol.*, **6**, 254-273.

Suszcynsky, D., A. Jacobson, J. Fitzgerald, C. Rhodes, E. Tech, and D. Roussel-Dupre, 2000: Satellite-based global lightning and severe storm monitoring using VHF receivers. *EOS, Trans. Am. Geophys. Union*, **81**, F91.

Suszcynsky, D. M. and M. J. Heavner, 2003: Narrow Bipolar Events as indicators of thunderstorm convective strength. *Geophys. Res. Lett.*, **30**, 1879, doi:10.1029/2003GL017834.

Toracinta, E. R. and E. Zipser, 2001: Lightning and SSM/I-ice-scattering mesoscale convective systems in the global tropics. *J. Appl. Meteor.*, **40**, 983-1002.

Toracinta, E. R., D. J. Cecil, E. J. Zipser, and S. W. Nesbitt, 2002: Radar, passive microwave, and lightning characteristics of precipitating systems in the tropics. *Mon. Wea. Rev.*, **130**, 802-824.

Ushio, T., S. J. Heckman, D. J. Boccippio, H. J. Christian, and Z.-I. Kawasaki, 2001: A survey of thunderstorm flash rates compared to cloud top height using TRMM satellite data. *J. Geophys. Res.*, **106**, 24,089-24,095.

Ushio, T., S. Heckman, K. Driscoll, D. Boccippio, H. Christian, and Z.-I. Kawasaki, 2002: Cross-sensor comparison of the Lightning Imaging Sensor (LIS). *Int. J. Remote Sensing*, **23**, 2703-2712.

Weinman, J. A. and P. J. Guetter, 1977: Determination of rainfall distributions from microwave radiation measured by the Nimbus 6 ESMR. *J. Appl. Meteorol.*, **16**, 437-442.

Wiedner, M., C. Prigent, J. R. Pardo, O. Nuissier, J.-P. Charboureau, J.-P. Pinty, and P. Mascart, 2004: Modeling of passive microwave responses in convective situations using output data from mesoscale models: Comparison with TRMM/TMI satellite observations. *J. Geophys. Res.*, **109**, D06124, doi:10.029/2003JD004280.

Williams, E. R., 1985: Large scale charge separation in thunderclouds. *J. Geophys. Res.*, **90**, 6013-6025.

— —, 2001: Chapter 13: The Electrification of Severe Storms. *Severe Convective Storms*, C. A. I. Doswell, Ed., American Meteorological Society.

Table 1: LASA stations in Florida (cumulative over 1999-2002).

station name (abbreviation)	longitude (deg E)	latitude (deg N)
Boca Raton (br)	-80.1015	26.3733
Cape Kennedy (kc)	-80.6424	28.5386
Tampa (ta)	-82.4145	28.0598
Fort Myers (fm)	-82.0151	26.6346
Gainesville (gv)	-82.3472	29.6424
near Fort Myers (fy)	-81.8687	26.6441
Orlando (or)	-81.1960	28.5860
Daytona (da)	-81.0472	29.1891
Tallahassee (te)	-84.2994	30.4461
Key West (kw)	-81.6899	24.5816

FIGURE CAPTIONS

Figure 1: The LASA study zone centered on 28 N, -81.5 E in central Florida. The 400-km-radius circle marks the zone within which LASA lightning locations are accepted for this study.

Figure 2: (a) VIRS 10.8-micron brightness temperature, and (b) TMI 85-GHz PCT (see text), for a single satellite pass over the LASA study region. Lightning events are overlaid in the images (small square symbols: ordinary lightning; large triangles: NBEs). The extensive cold cloud top (in 2a) contains only a much smaller area of intense convection as revealed in the PCT (in 2b). The lightning events of both type are localized on the intense convection.

Figure 3: Statistical distributions of VIRS 10.8-micron cloud-top temperature. Each curve is separately normalized to unity, for ease of comparison. Thin solid curve: All pixels, regardless of lightning. Thick solid curve: Only those pixels within 30 km of each non-NBE lightning event. Thick dashed curve: Only those pixels within 100 km of each non-NBE lightning event.

Figure 4: Similar to Figure 3, but for NBEs.

Figure 5: Similar to Figure 3, but with the heavy curves showing the distribution of the *coldest pixel* within 30 km (heavy solid curve) and within 100 km (heavy dashed curve) of non-NBE lightning events.

Figure 6: Similar to Figure 4, but with the heavy curves showing the distribution of the *coldest pixel* within 30 km (heavy solid curve) and within 100 km (heavy dashed curve) of NBEs.

Figure 7: Separately normalized distributions of VIRS 10.8-micron brightness temperature. Dashed curve shows all pixels in all scenes. Solid curve shows the same data, but after removing all pixels that are within 30 km of any LASA lightning event.

Figure 8: Statistical distributions of TMI 85-GHz PCT (see text). Each curve is separately normalized to unity, for ease of comparison. Thin solid curve: All pixels, regardless of lightning. Thick solid curve: Only those pixels within 30 km of each non-NBE lightning event. Thick dashed curve: Only those pixels within 100 km of each non-NBE lightning event.

Figure 9: Similar to Figure 8, but for NBEs.

Figure 10: Similar to Figure 8, but for the coldest 85-GHz PCT within 30 km (heavy solid curve) and 100 km (heavy dashed curve) of non-NBEs. Light solid curve is for the entire set of scene pixels.

Figure 11: Similar to Figure 10, but for NBEs.

Figure 12: Separately normalized distributions of TMI 85-GHz PCT. Dashed curve shows all pixels in all scenes. Solid curve shows the same data, but after removing all pixels that are within 30 km of any LASA lightning event.

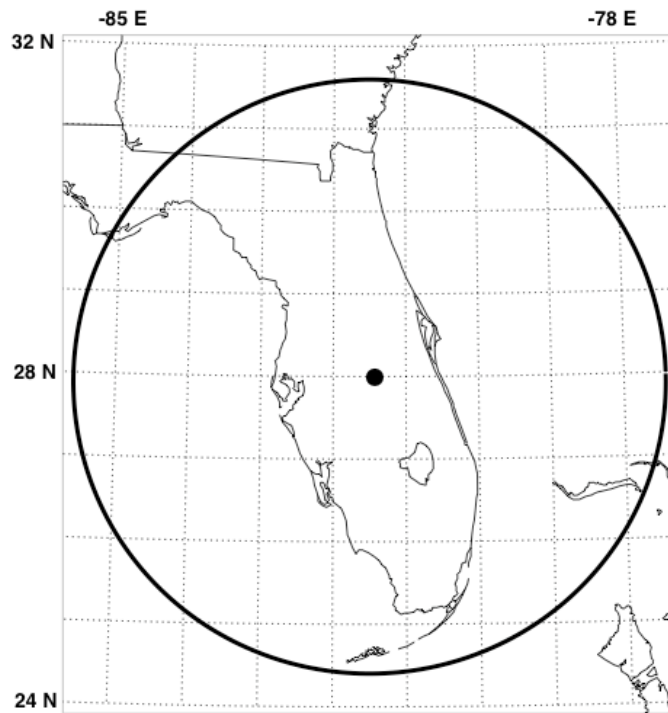


Figure 1: The LASA study zone centered on 28 N, -81.5 E in central Florida. The 400-km-radius circle marks the zone within which LASA lightning locations are accepted for this study.

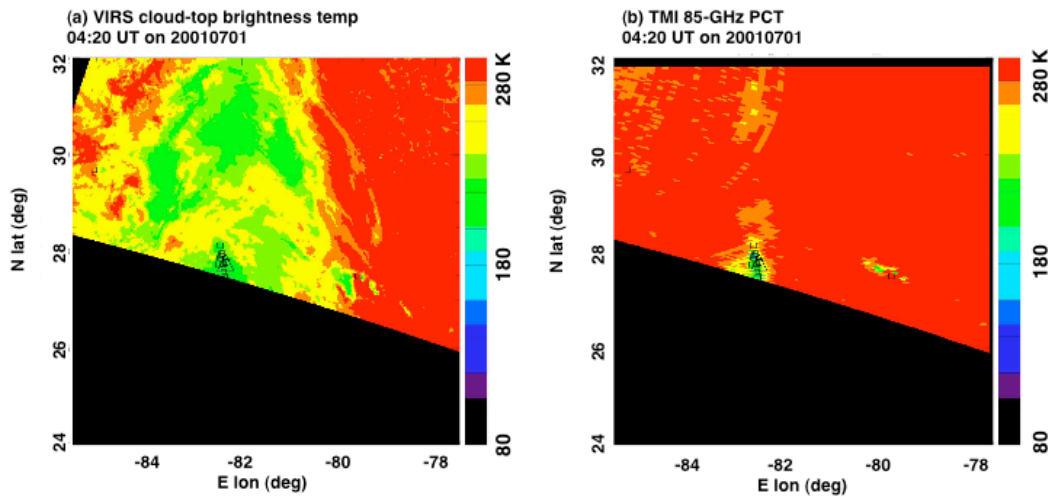


Figure 2: (a) VIRS 10.8-micron brightness temperature, and (b) TMI 85-GHz PCT (see text), for a single satellite pass over the LASA study region. Lightning events are overlaid in the images (small square symbols: ordinary lightning; large triangles: NBEs). The extensive cold cloud top (in 2a) contains only a much smaller area of intense convection as revealed in the PCT (in 2b). The lightning events of both type are localized on the intense convection. The lightning events of both type are localized on the intense convective core.

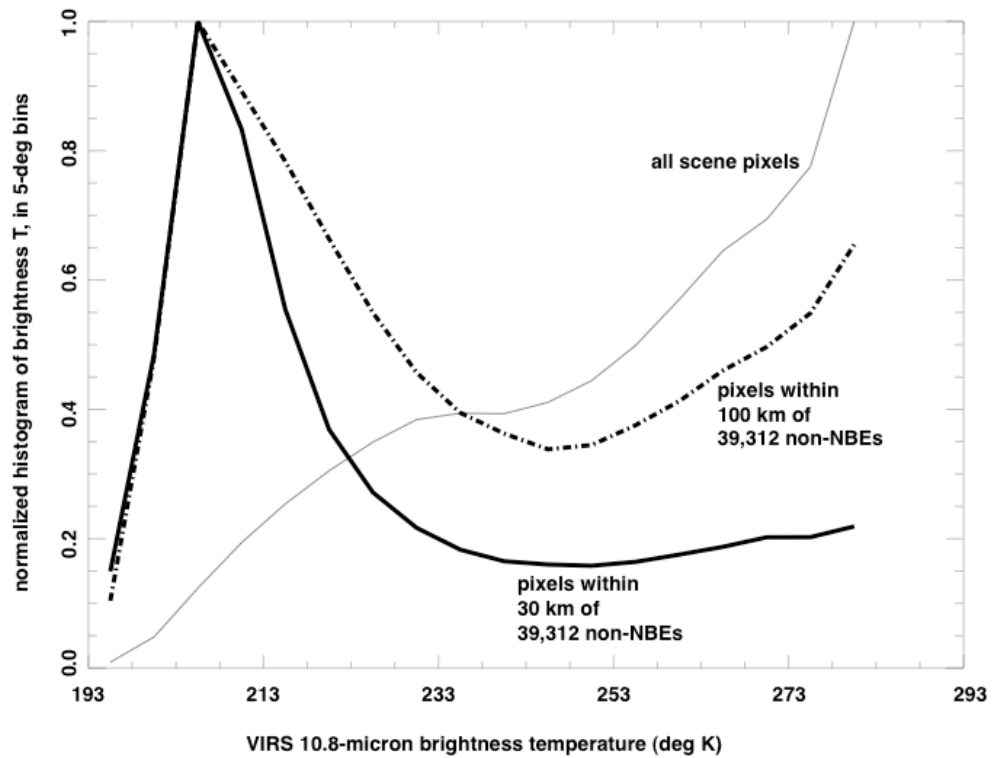


Figure 3: Statistical distributions of VIRS 10.8-micron cloud-top temperature. Each curve is separately normalized to unity, for ease of comparison. Thin solid curve: All pixels, regardless of lightning. Thick solid curve: Only those pixels within 30 km of each non-NBE lightning event. Thick dashed curve: Only those pixels within 100 km of each non-NBE lightning event.

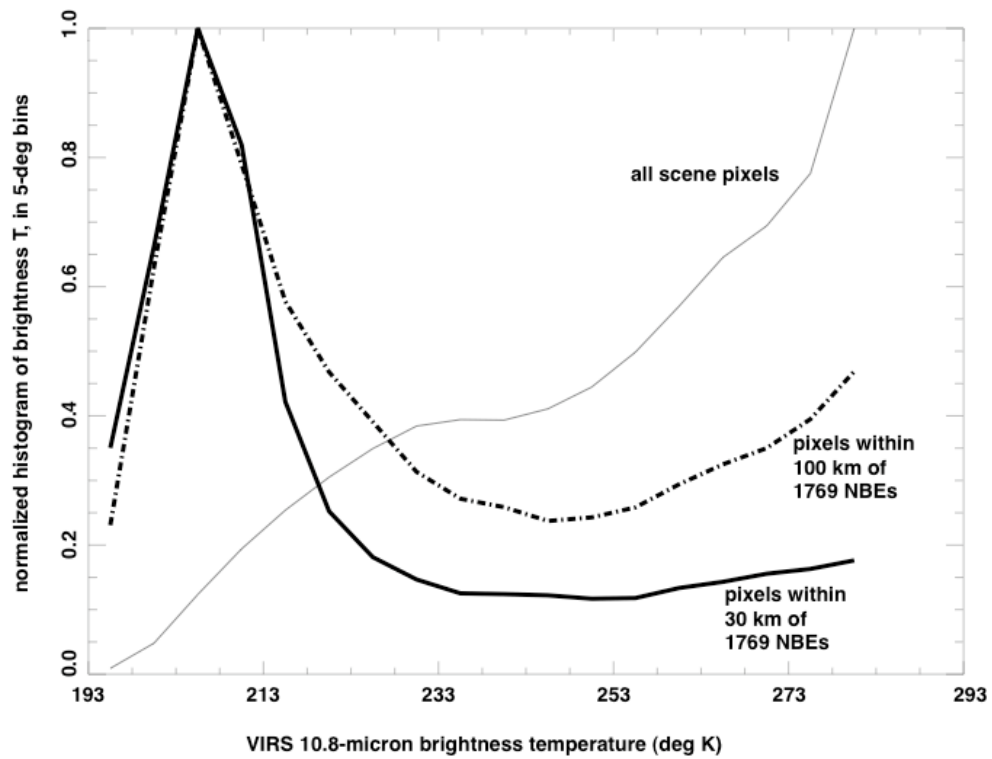


Figure 4: Similar to Figure 3, but for NBEs.

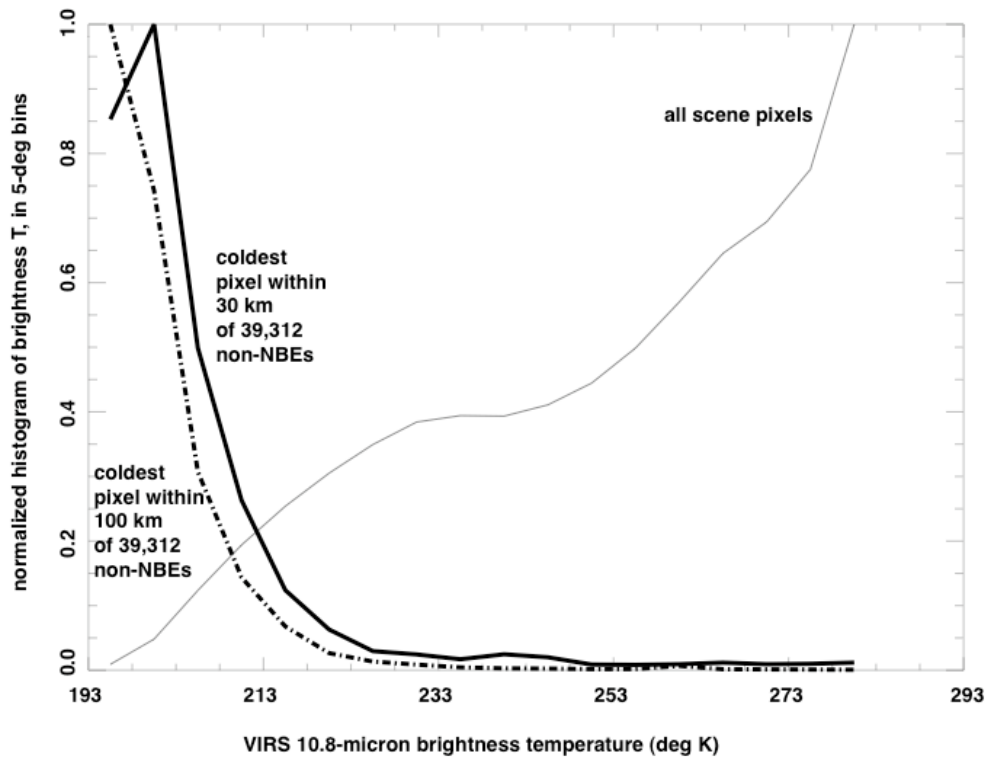


Figure 5: Similar to Figure 3, but with the heavy curves showing the distribution of the *coldest pixel* within 30 km (heavy solid curve) and within 100 km (heavy dashed curve) of non-NBE lightning events.

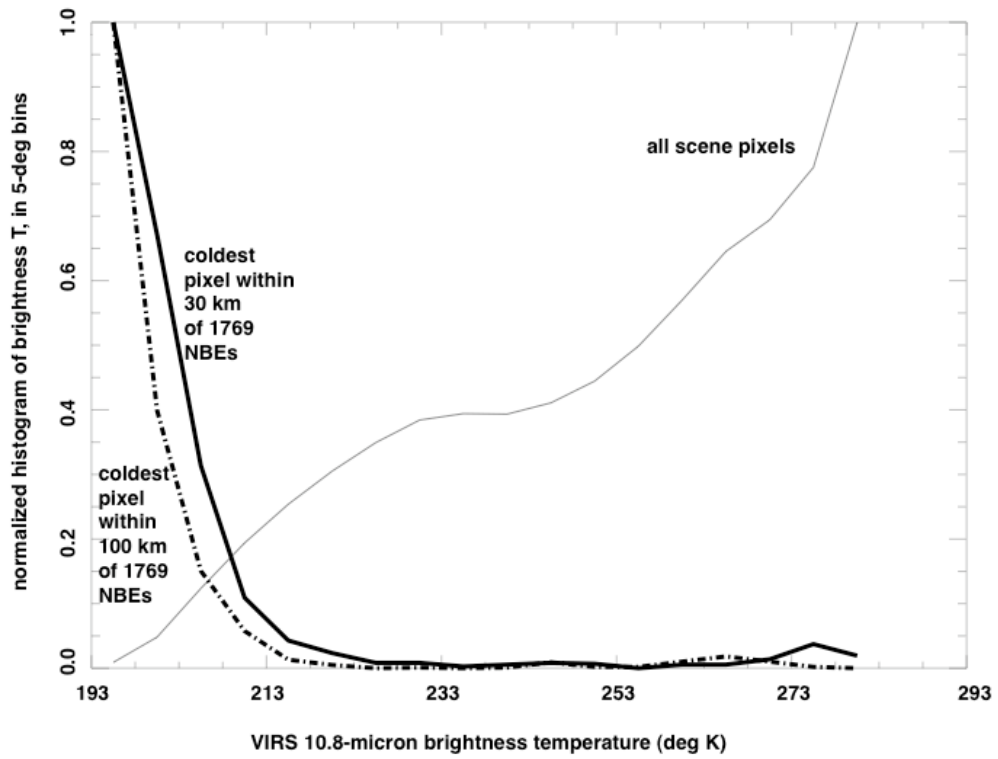


Figure 6: Similar to Figure 4, but with the heavy curves showing the distribution of the *coldest pixel* within 30 km (heavy solid curve) and within 100 km (heavy dashed curve) of NBEs.

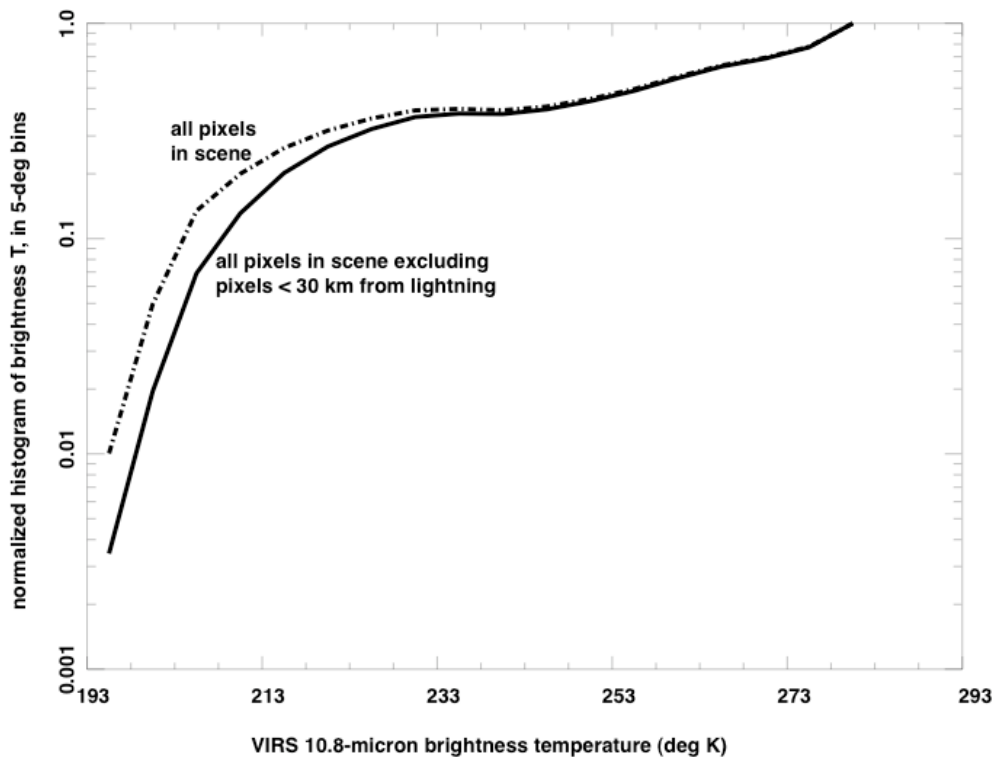


Figure 7: Separately normalized distributions of VIRS 10.8-micron brightness temperature. Dashed curve shows all pixels in all scenes. Solid curve shows the same data, but after removing all pixels that are within 30 km of any LASA lightning event.

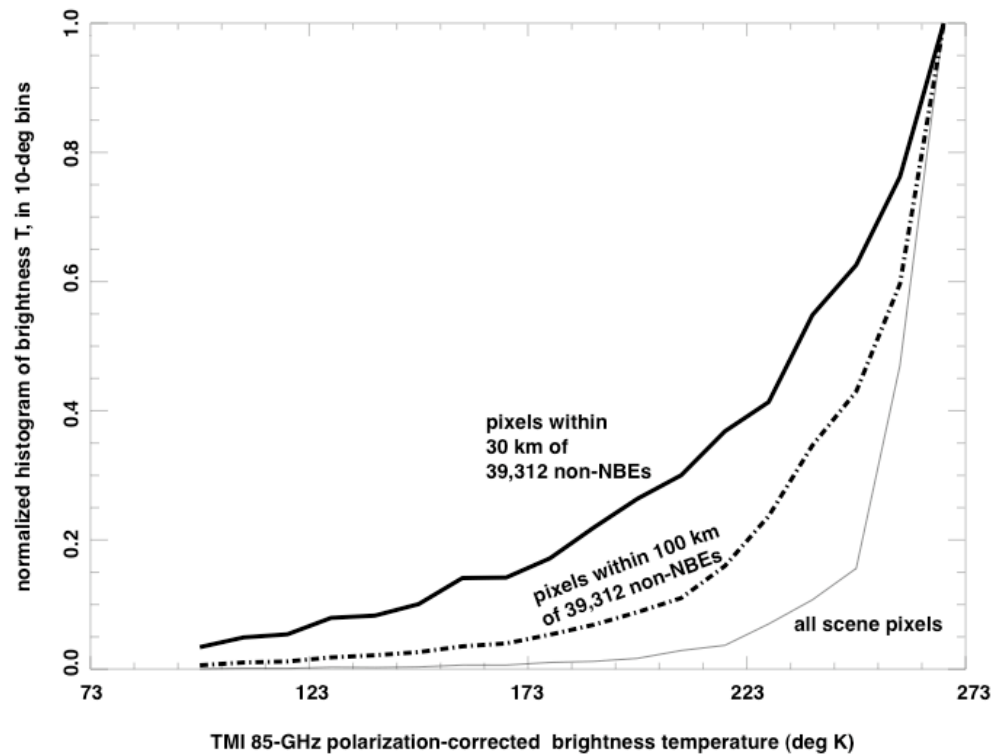


Figure 8: Statistical distributions of TMI 85-GHz PCT (see text). Each curve is separately normalized to unity, for ease of comparison. Thin solid curve: All pixels, regardless of lightning. Thick solid curve: Only those pixels within 30 km of each non-NBE lightning event. Thick dashed curve: Only those pixels within 100 km of each non-NBE lightning event.

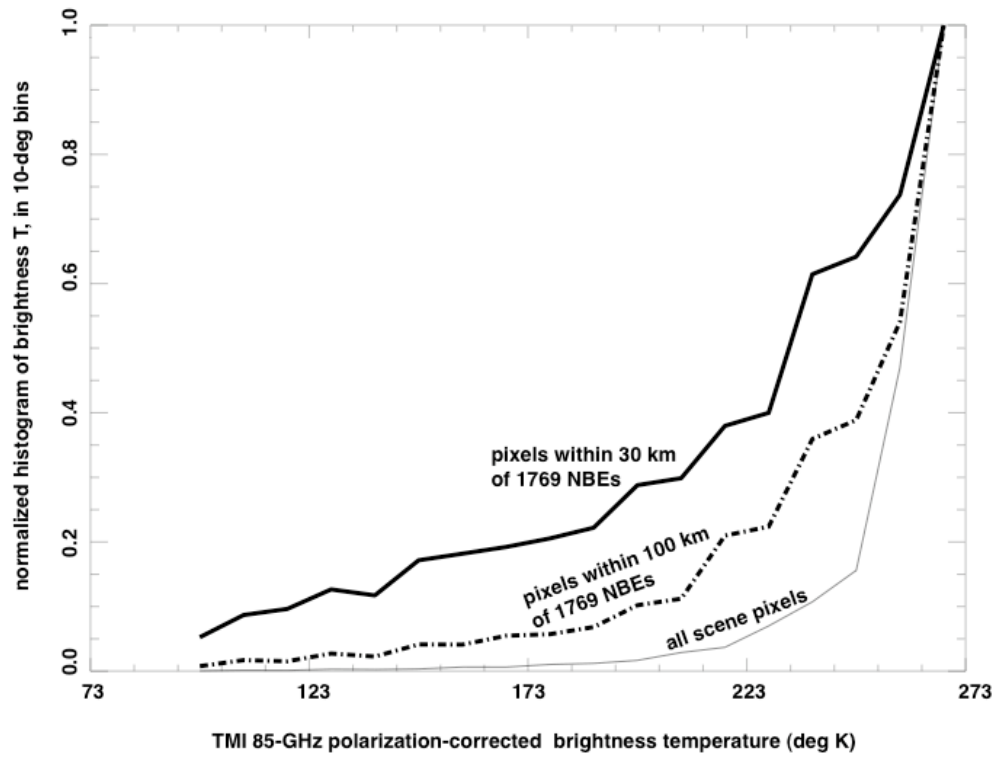


Figure 9: Similar to Figure 8, but for NBEs.

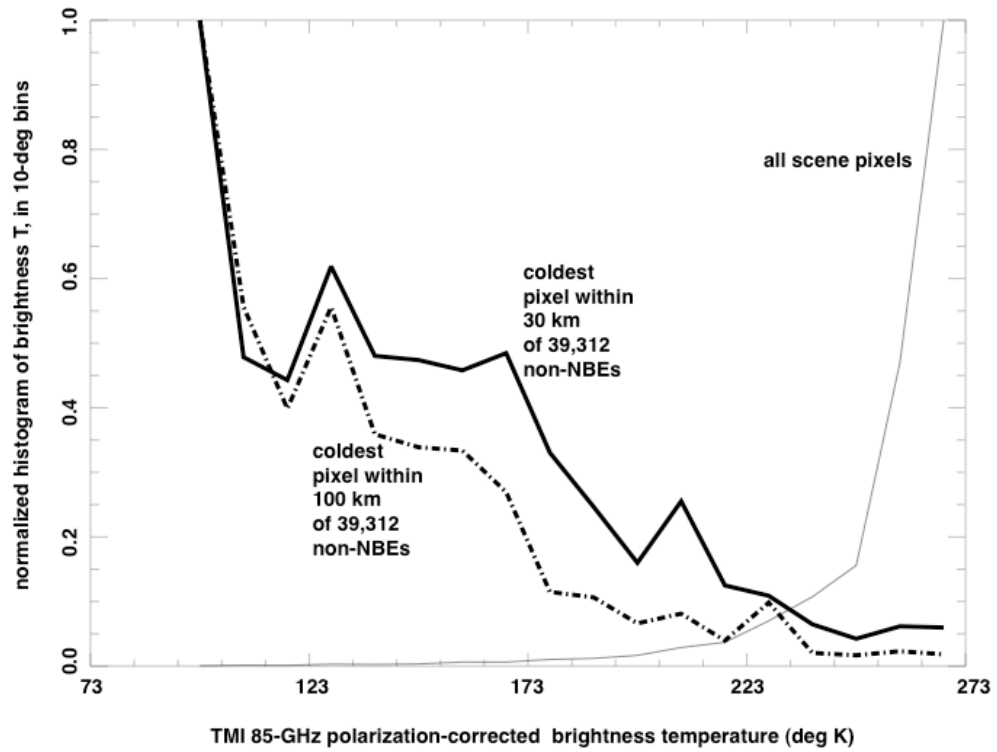


Figure 10: Similar to Figure 8, but for the coldest 85-GHz PCT within 30 km (heavy solid curve) and 100 km (heavy dashed curve) of non-NBEs. Light solid curve is for the entire set of scene pixels.

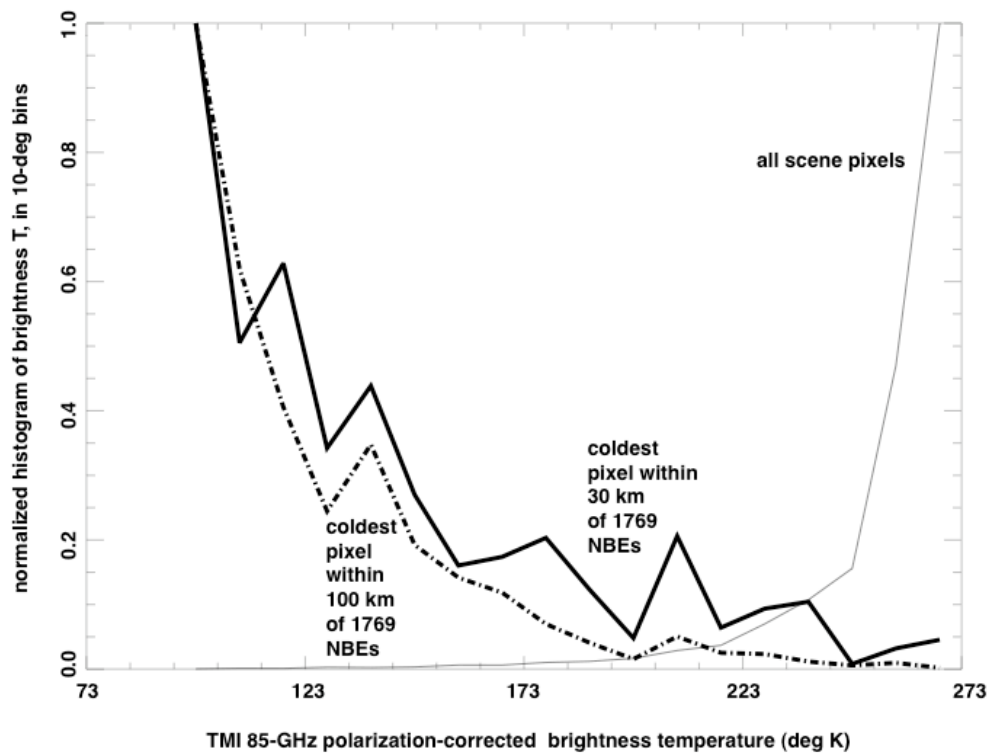


Figure 11: Similar to Figure 10, but for NBEs.

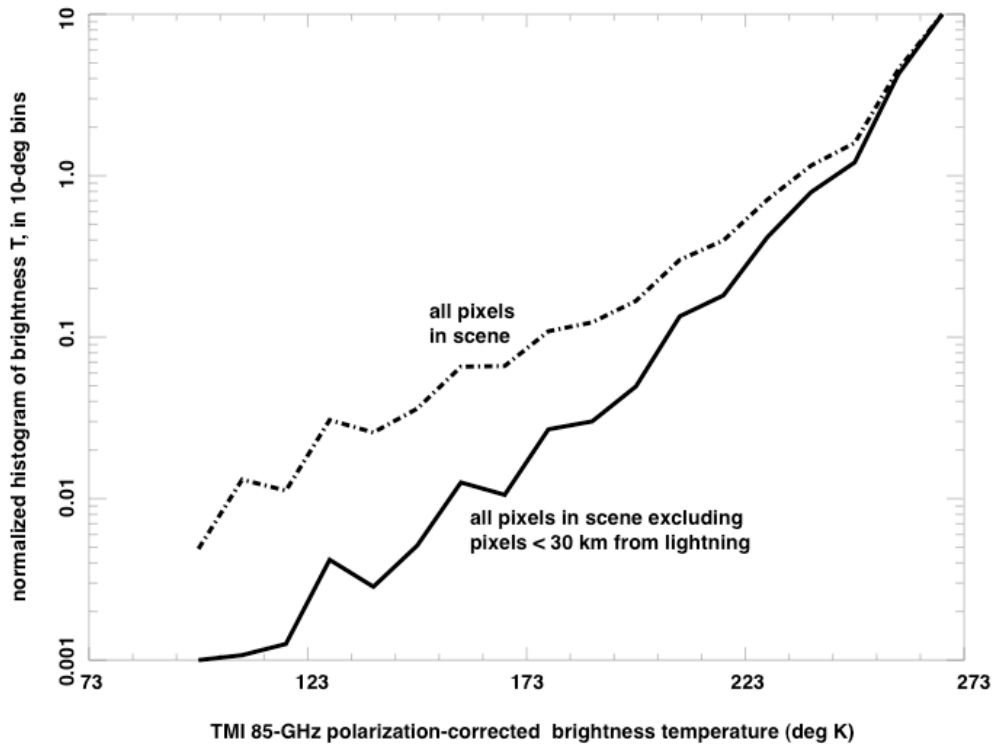


Figure 12: Separately normalized distributions of TMI 85-GHz PCT. Dashed curve shows all pixels in all scenes. Solid curve shows the same data, but after removing all pixels that are within 30 km of any LASA lightning event.